Spatiotemporal characteristics of TOMS-based dust aerosol optical depth in northern China during 1978–2005

Xiaoyu Ren, Yun Xie & Guoyu Ren

Earth Science Informatics

ISSN 1865-0473
Volume 10
Number 1

Earth Sci Inform (2017) 10:41-53
DOI 10.1007/s12145-016-0277-z

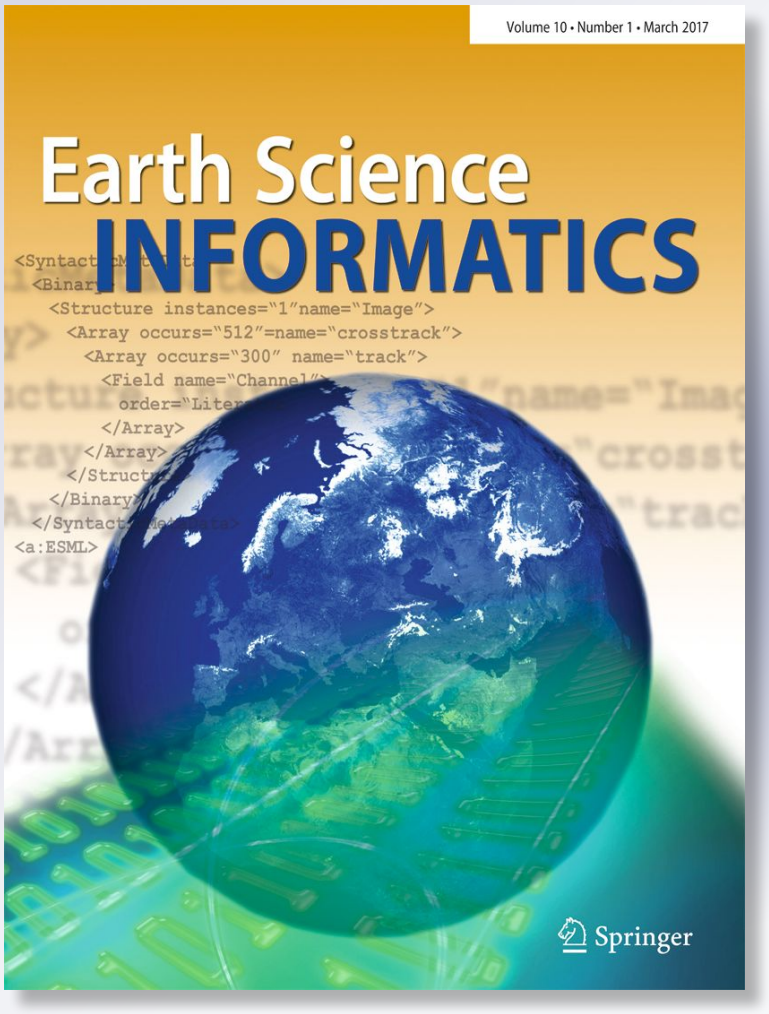

Springer

Earth Sci Inform (2017) 10:41–53
DOI 10.1007/s12145-016-0277-z

RESEARCH ARTICLE

Spatiotemporal characteristics of TOMS-based dust aerosol optical depth in northern China during 1978–2005

Xiaoyu Ren[1,2] · **Yun Xie**[1] · **Guoyu Ren**[2,3]

Received: 30 March 2016 / Accepted: 18 October 2016 / Published online: 27 October 2016

Abstract Using the Total Ozone Mapping Spectrometer (TOMS) data from the National Aeronautics and Space Administration (NASA) earth satellites, the Aerosol Optical Depth (AOD) as indicated by AOD Index (AI) for the period 1978–2005 is analyzed for northern China. The spatial distribution of annual mean AI has the largest values in the desert regions of northwestern China, such as southern Xinjiang Taklimakan Basin, western Gansu and Qinghai's Qaidam Basin. Large values are found in western Inner Mongolia, the Jogger Basin, and north of the Loess Plateau, as well as in the North China and Northeast China Plains. In Northern China, the AI of spring and summer is larger than in other seasons. The large AI values in spring register the most extensive coverage, but the AI values in regions affected by the Asian monsoon experience a significant decrease during the summer season. The lowest AI values generally occur in autumn in North and Northeast China, but they appear in winter in the northwestern arid region. Overall, the analysis results using TOMS AI data well reflect the spatiotemporal characteristics of dust aerosol as reported previously based on the dust weather observation data, with greater consistency seen in northwestern arid and semi-arid regions. It is also realized that the TOMS AI data are potentially useful for estimating atmospheric mineral aerosol deposition flux in northern China in order to better understand the formation and evolution of China loess in the Quaternary.

Keywords Aerosols · Dust storm · Northern China · Aerosols optical depth · Seasonal variation · Spatial pattern

Communicated by: H. A. Babaie

✉ Guoyu Ren
guoyoo@cma.gov.cn

[1] School of Geography, Beijing Normal University, Beijing 100875, China

[2] Department of Atmospheric Science, School of Environmental Studies, China University of Geosciences, Wuhan 430074, China

[3] Laboratory for Climate Studies, National Climate Center, China Meteorological Administration, Beijing 100081, China

Introduction

Dust weather is a type of low-visibility phenomenon that happens in arid and semi-arid areas. Factors affecting the formation of dust weather include strong winds, dust sources and unstable weather conditions (Wang et al. 1996; Qiu et al. 2001). Dust weather in China mainly occurs in the northern region and most frequently in the northwest arid regions (Wang et al. 2000; Zhou 2001; Fang et al. 2001, 2003; Ding and Liu 2011; Yang et al. 2012. Dust weather can lead to natural disasters, influence human health, modify regional climate through change in atmospheric aerosol concentrations, and exert an important impact on global biogeochemical processes (Novakov and Penner 1993; Zhuang et al. 2001; Wang et al. 2012; Seinfeld and Pandis 2016) .

From the perspective of the environment and the evolutionary history of the Quaternary, dust weather, as an important geologic agent, has been assumed to cause the deposition of loess in China's northern region. Many researchers have addressed the connections between material sources, transmission paths, and settling flux causing loess deposition from various angles of view. The main source of loess deposition in China was assumed to come from the Gobi Desert in central Asia in the spring (Liu 1985; Pye and Zhou 1989; Zhang et al. 1993; Ding et al. 1999; Sun et al. 2001). Previous studies also addressed the modern spatiotemporal distribution of dust weather and the evolution of seasonal atmospheric circulation

(Wang et al. 2003; Fang et al. 2003; Zhang and Ren 2003; Fan and Wang 2006; Ding and Liu 2011; Yang et al. 2012). Meteorological ground stations are used to analyze dust weather through instantaneous wind speed and visibility in China (Wang and Ren 2003; Qian et al. 2004), and the individual dust weather processes are monitored by satellite remote sensing. However, ground-based observation data and related research have inherent defects. These data cannot accurately reflect the average annual and seasonal mass fluxes within the entire atmosphere. The lower troposphere contains a certain amount dust material that, because of dust devils or wind gusts, does not reach the standard of "dust weather". At the same time, the ground stations cannot measure the actual thickness of dust in the atmosphere, and the records cannot reflect the actual Aerosol Optical Depth (AOD) of dust or the deposition flux due to the differences in terrain height and vertical transmission intensity.

Dust AOD is inverted by the near-infrared or visible light spectrum detected by satellites (Chu et al. 2002; Levy et al. 2007). For example, AOD can be obtained through the Multi-angle Imaging Spectra-Radiometer (MISR) based on the Earth Observing System (EOS), but MISR has no ability to distinguish between dust aerosols, sulfate aerosols and biomass burning aerosols (Martonchik et al. 2002). Total Ozone Mapping Spectrometer (TOMS) carried by the Nimbus 7 Meteor 3 and Earth-Probe could be used to deliver data of dust and carbonaceous AOD almost covering the entirety of the world's oceans and lands. The data set better represents the actual content of dust aerosols in areas dominated by different types of aerosols, and the usefulness has been verified by comparison with the Aerosol Robotic Network (AERONET) (Torres et al. 1998, 2002).

Washington et al. (2003) found that the Sahara Desert is the world's most important source of atmospheric dust aerosols, along with the Taklimakan Desert in China, by analyzing TOMS AOD data. Deng et al. (2009) pointed out that dust storms, dust devils and dry heat convection mutually impact the content of mineral aerosol in deserts, through analyzing dust aerosol content in northwest China using TOMS AOD data. Researchers have also studied China's other regions applying the same data (Li et al. 2003; Xu et al. 2002; Streets et al. 2001, 2008; Mi et al. 2007; Lin et al. 2007). However, existing studies generally focus on dust weather, dust AOD distribution, and comparisons with the ground meteorological observation records. Analysis of the basic climatologic features of dust aerosols in North China is rare, particularly in connection with Quaternary loess deposition.

This paper analyzes the tempo-spatial characteristics of dust AOD of northern China using the AI derived from AOD dataset. The results are helpful for further understanding of dust climatology in northern China and the geological role of dust aerosol in the process of loess deposition.

Data and methods

Data

Daily grid data of TOMS AOD from Nimbus (1978–1993) and Earth-Probe (1996–2005) was used. The grid size is 1.00° × 1.25°. The missing data in 1994 and 1995 due to technique problems of satellite was replaced by the annual average of the years with records.

TOMS absorbs ultraviolet radiation (UV) with high sensitivity to clearly separate dust and carbon aerosols from sulfate and sea-salt aerosols. TOMS AOD data reveal dust aerosol optical depth using the contrast relations of backscattering wavelengths depending on the TOMS observation records. The dataset is thus regarded to mainly indicate optical depth of dust aerosol in the atmosphere, including carbon aerosols from industrial, transportation, fire, and straw burning sources (Torres et al. 2002; Washington et al. 2003). At present, it is difficult to isolate dust aerosol from carbonaceous aerosol through passive remote sensing; that is to say, we can hardly attain the high resolution and long-period dust aerosol data that fully reflect the content of dust aerosols in the atmosphere.

Dust weather surface observation data were used for comparison with the AOD data, but the resulting figures and tables were not exclusively shown here because they were previously published (Ren et al. 2014). The weather data are from National Meteorological Information Center, China Meteorological Administration, which includes number of days with dust weathers for time period 1978–2005. Dust weathers in the observational dataset are further divided into three categories according to the observational visibility and instantaneous wind speeds: sandstorms, suspended dust and blowing sand (Ye et al. 2000; Qian et al. 2002; Wang and Ren 2003). Dust weather frequency is the sum of occurrence days of the three categories of dust events.

Method

In this paper, the study area was defined as the region north of latitude 30°N in mainland China. The area was divided into three sub-regions of Northeast China, North China and Northwest China. Almost all inland deserts, sandy lands, and steppes are located in this area, and the most frequently occurred dust weathers are also found in the study area. In Northwest China especially in the Taklimakan basin and western Gansu and Inner Mongolia, the climate is characterized by extremely low precipitation of less than 80 mm and annual mean numbers of sandstorms, suspended dust and blowing sand reach about 20 days, 50 days and 30 days respectively. North China has less dust weathers, and Northeast China has the least frequency of dust weather events. In both North China and Northeast China, the dust events frequencies all increase from southeast to northwest (Wang and Ren 2003) (Fig. 1) .

Grid averaged values were obtained for pentad, monthly, quarterly, and annual intervals from AOD dataset between 1978 and 2005. Area averages were calculated from the grid averaged monthly, seasonal, and annual values using the simple arithmetic-average method. Due to the smaller latitude span, the calculation results by using the simple arithmetic-average method and the latitude and longitude grid area weighted-average method bear almost no difference. On this basis, the new time series called AOD Index (AI) for individual grids, three sub-regions and the whole study area were thus obtained for pentad, monthly, quarterly, and annual means by using the simple arithmetic-average method.

Seasons have been divided based on climatological definition: spring for March, April and May; summer for June, July and August; autumn for September, October and November; winter for December, January and February. One year is divided into 72 pentads, with each pentad being five days or six days (final pentads of months 1, 3, 5, 7, 8, 10, and 12 are six days) and the last pentad of February four days.

Method of Empirical Orthogonal Functions (EOF) was used to examine the spatial characteristics of dominant modes of AI data and the associated temporal variation in the study region. The EOF analysis was conducted on the covariance matrix of the AI data. Because of satellite replacement, observations were heterogeneous over time; this may impact the analysis of the long-term trends, but it will have less impact on climatological characteristics of the dust aerosol.

Results

Spatial characteristics

Figure 2 shows the distribution of annual mean AI in northern China from 1978 to 2005. The highest AI values more than 0.8 are located in desert regions, such as the Taklimakan basin, west of Gansu and the Qaidam Basin; the second highest value is in the western part of Inner Mongolia, where AI is generally between 0.5 and 0.8. The AI in Junggar Basin of Xinjiang, north of the Loess Plateau, the North China Plain, and the Northeast China Plain is relatively high, usually between 0.4 and 0.7. The AI averages are less than 0.2 in the border area of Sichuan, Qinghai, and Tibet; Altai and west of the Tianshan Mountains have an AI less than 0.2. Most of the Tibetan Plateau, the Tianshan Mountains, the Altai Mountains, the Qinling Mountains, the Daba Mountains, lower reaches of the Yangtze River basin, the Taihang Mountains, the Great and Lesser Khingan Mountains, and the Changbai Mountains, all have a relatively low AI value.

The region that sees the highest average annual AI is in the center of the Taklimakan Desert, which has an extremely dry climate, and the highest frequency of dust weather in northern China. Western Inner Mongolia, the northern Loess Plateau, the northwest Qaidam Basin, and the Horqin Sandy Land of central Northeast China are also prone to dust weather (Zhou 2001; Wang et al. 2003; Wang and Ren 2003). Overall, the annual mean AI gradually increases from the southeast to the northwest, indicating a generally lower value in the monsoon region and a usually higher value in the arid and sub-arid non-monsoon region. The observational studies also show that, in the southeastern parts of the study region, the stronger (weaker) winter (summer) monsoon benefits the occurrence of dust weather in winter and the next spring, and the stronger (weaker) summer (winter) monsoon suppresses the occurrence of dust weather (Ye et al. 2000; Wang et al. 2000; Wu et al. 2010). The mechanism for the association is because the strong winter monsoon can bring less precipitation in northern China, and the strong summer monsoon can generally cause higher than normal precipitation in the study region (Ye et al. 2000; Wang et al. 2000, 2003; Fang and Wang 2003).

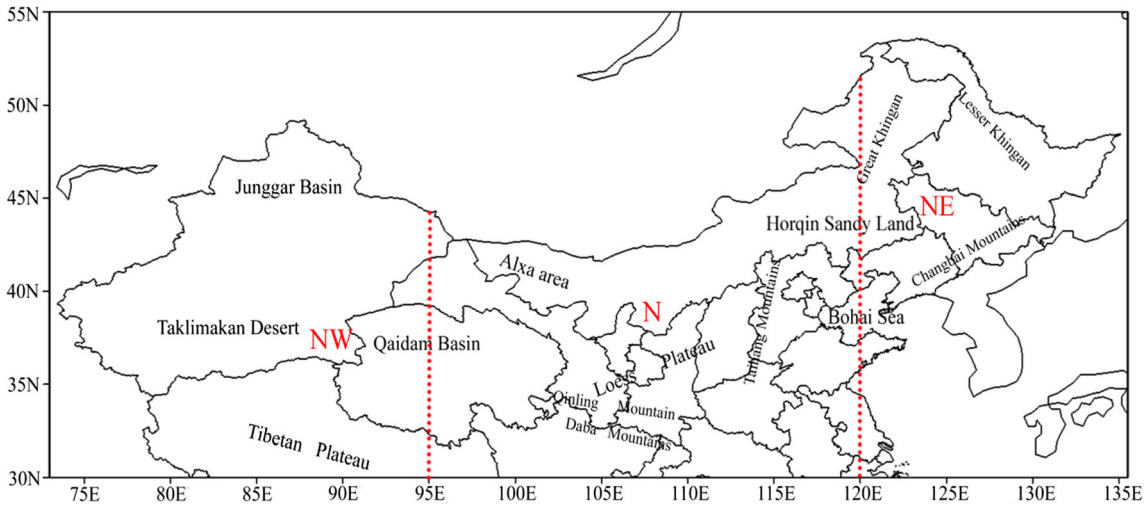

Fig. 1 Location of the study area and the three sub-regions

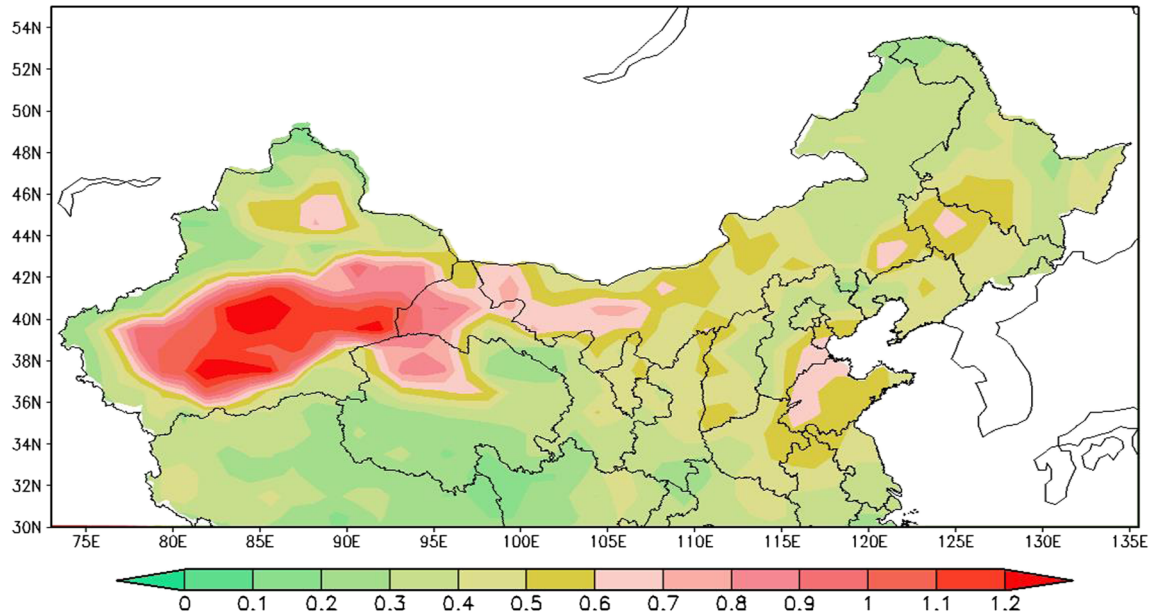

Fig. 2 Distribution of annual mean AI in northern China for the period 1978–2005

In the North China Plain, however, there is also a zone of relatively high annual mean AI, which does not exactly match the area of dust weather frequency (Wang and Ren 2003). The likely reason for this is the greater addition of carbonaceous aerosols emitted by anthropogenic sources in the North China Plain. The main sources of carbonaceous aerosols are natural sources (forest fires and grassland fires) and anthropogenic sources. Anthropogenic sources include residential sources (fossil fuels and biofuels) and industrial sources. Compared with anthropogenic sources, carbonaceous aerosol emissions of natural sources are largely negligible (Bond et al. 2004; Lu et al. 2011; Zhang et al. 2013a). The coal burning including coal-fired for heating in winter is the main source of carbonaceous aerosol emissions. In the crop harvest season, emissions of straw burning and other biomass combustion are also the important source of carbonaceous aerosols (Li et al. 2007; Zhang et al. 2009; Wang et al. 2011; Zhang et al. 2013b). The North China Plain is one of the largest areas of carbonaceous aerosol emissions in China (Wang et al. 2011). The aerosol emissions, including the carbonaceous aerosol emissions, may have also been the main reason for the significant decline in daylight and solar radiation in this area for the last 50 years (Ren et al. 2005).

Relatively high values of the Northeast China Plain are related to frequently occurred dust weathers in the Horqin Sandy Land, in spite of the fact that the anthropogenic carbonaceous aerosol emissions in wintertime are also important in central urban belt of the region. The area is located in higher latitude, and the coal usage for heating in winter is the largest in China. Therefore, the contribution from the anthropogenic carbonaceous aerosol emissions to the high AI values in the Northeast China Plain would be also important (Wang et al. 2011).

The influence of terrain on distribution of annual mean AI is obvious. The AI values in plains and basins appear relatively high, whereas the plateau and mountain areas often show a relatively low value. The reason for the spatial difference is that dust AOD, as reconstructed by satellite data, depends on not only the concentration of atmospheric aerosols near the surface, but also the thickness of aerosol-containing air or atmospheric column in the troposphere. In the plains and basins, the atmosphere rich in aerosols is thicker, and AI value is higher; in the plateaus and mountains, however, the lesser thickness of the atmosphere rich in aerosols makes the AI values lower. Relatively high AI values distributed in the northern and northeast plains are also related to the terrain factor. Therefore, the AI characterizes the dust deposition flux more precisely than the frequency of dust weather events, because both the manual observation and Autonomous Weather Station (AWS) observation are made near the surface, and they can hardly reflect the complete dust content of the entire atmosphere.

Figure 3 shows the distribution of seasonal mean AI for period 1978–2005. As a whole, mean AI in the spring and summer of northern China was significantly higher than in the other seasons, and the distribution areas of high AI values are consistent with the high incidence of dust weather (Ren et al. 2014). The seasonal mean AI of the Taklimakan Desert, the Qaidam Basin, and the Alxa area in spring and summer remained at 0.8, and they register the largest seasonal dust AOD of all seasons.

The highest frequency of occurrence of dust weather well corresponds to the high-value AI areas in the spring (Fig. 3a) (Ren et al. 2014). The spatial distribution of seasonal mean AI in spring is similar to annual mean AI, indicating that dust weather in the spring is the greatest contributor to annual mean AI. The relatively high spring mean value in the North and

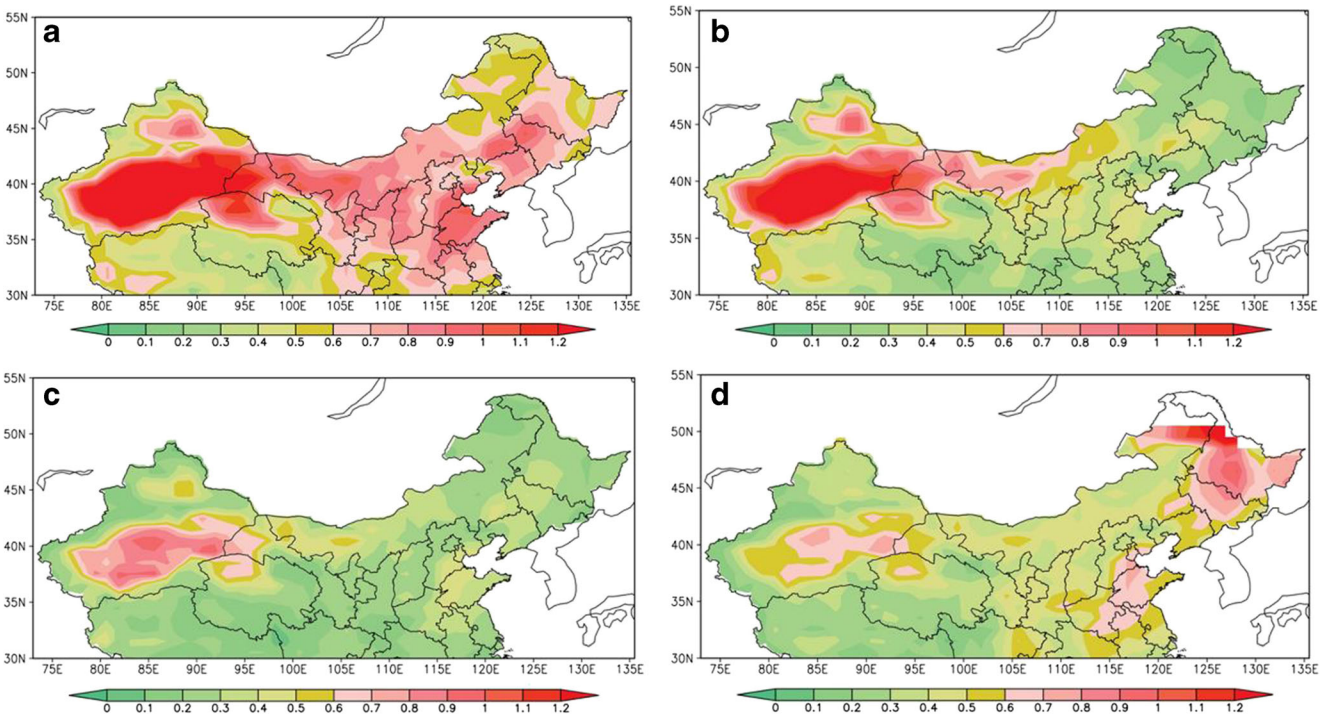

Fig. 3 Distribution of seasonal mean AI in northern China for the period 1978–2005. **a**, **b**, **c**, **d** represent spring, summer, autumn and winter respectively

Northeast China Plains may result from the combined influences of dust weather, emissions of carbonaceous aerosols and lower terrain. The smallest AI values in spring are located in the eastern Tibetan Plateau and western Junggar Basin where seasonal mean AI values are as low as 0.2.

Compared to the spring, the greatest change in the spatial distribution of seasonal mean AI in summer occurs in North China and Northeast China (Fig. 3b). The strength of secondary high-value centers decreases significantly and the scope shrinks. It may be related to a decrease in the frequency of dust weather, which is caused by the increase in precipitation, the rising soil-water content and the recovery of vegetation due to the prevailing summer monsoon. In the summer, the ranges of seasonal mean AI in the Taklimakan Basin, the Qaidam Basin and Alxa area have been reduced, but not so significantly, and the strength of the center is hardly diminished. Meteorological observations also reveal that the peak of dust-weather frequency in the Taklimakan Basin occurs from June to July (Wang et al. 2003; Wang and Ren 2003; Li et al. 2006), but the summer AI high values from satellite remote sensing are more obvious. It may be related to locally convective activity from the desert surface and frequent dust devils in the summer (Deng et al. 2009). These local, short-term, high-frequency dust events are of great significance for the increase in dust AOD in the atmosphere, but they have seldom been recorded by the ground observations according to the current operational criteria. Several small values are evident in summer along the border of the Tibetan Plateau and the Sichuan Basin, in north of the Great Khingan Mountains, the Lesser Khingan Mountains, northeast of the Changbai Mountains, the Altai Mountains and other regions of humid regions.

Autumn witnesses the lowest seasonal mean AI values, mostly below 0.3 (Fig. 3c). The areas of high values in the spring and summer have narrowed, but the lower value areas in the eastern Tibetan Plateau, north of Northeast China have expanded significantly. To most regions, autumn represents a low incidence of dust weather frequency (Wang and Ren 2003; Fan and Wang 2006), and the seasonal mean AI values are generally low, except for the Taklimakan Basin and the surrounding areas. The seasonal mean AI values of the Taklimakan Desert in autumn are lower than those in spring and summer, but generally higher than those of winter.

The seasonal mean AI values in the winter are relatively low in most parts of northern China, including the arid areas of Northwest China (Fig. 3d). However, the mean AI of the monsoon region in winter is significantly higher than in summer and autumn, especially in the Northeast China Plain. The possible reason is the tremendous increase in emission of carbonaceous aerosols by anthropogenic sources due to the energy consumption for heating (Zhang et al. 2009; Wang et al. 2011). The unique weather and climatic condition in winter would be also important. The vertical gradient of the near surface air temperature characterizes the stratification stability of the atmosphere in calm weather condition in winter, and the high carbonaceous aerosol in the lower atmosphere emitted due to heating and traffic is not easy to diffuse because of the lower-tropospheric temperature inversion, resulting in the higher carbonaceous AOD in the season in the densely

populated areas (Gao et al. 2009). It is also possible that the persistent snow cover in the season somehow affects the monitoring accuracy of TOMS (Torres et al. 2002).

Seasonal change

Figure 4 shows the seasonal change for AI from 1978 to 2005. In Northern China on a whole, the months of high values appear in the spring and early summer (March to June), with the highest value (>0.6) in April and May; the lowest value appears in autumn (September–November) (Fig. 4a). The monthly mean AI is less than 0.3, and only 0.25 in October; winter is the second season with high AI values, following those in spring, and the values in January and February are greater than 0.4. Summer is the second low-value season after autumn, and the monthly mean AI values decline from June to August. Autumn registers minimum values of a year. The seasonal change in monthly mean AI and ground-based observations of dust weather frequency shows a good consistency. The occurrence of dust weather events in ground observation data is in peak in April and May, however, and the period of the lowest frequency is from August to November.

Figure 4b shows seasonal variations in region-averaged pentad mean AI, which reflects more detailed structure of the seasonal variation. The whole study area enters a period of rapid growth from the tenth pentad until the twenty-fifth pentad when it peaks, and then decreases to the lowest value at a rapid rate until the fifty-seventh pentad, followed by a slow

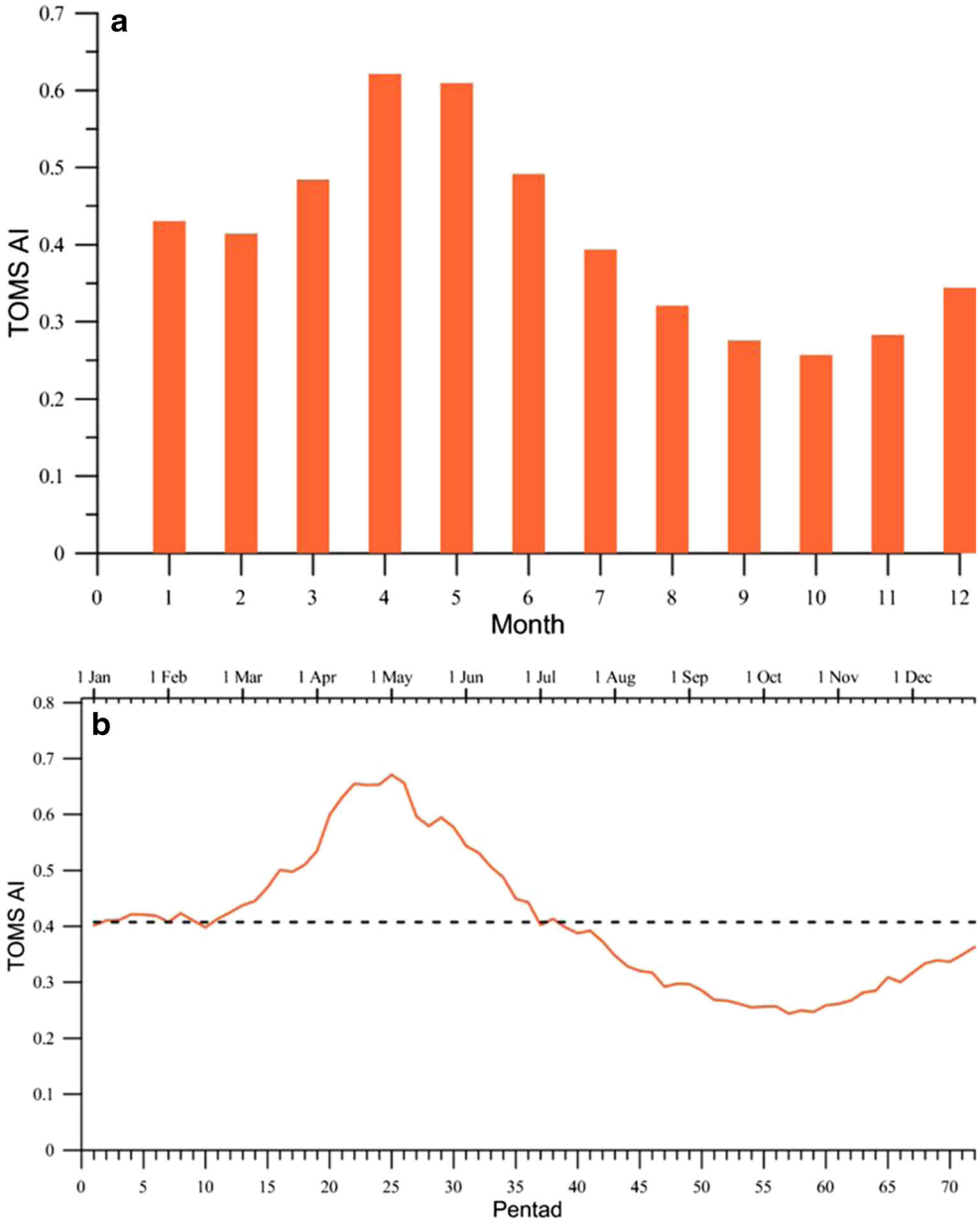

Fig. 4 Seasonal variations in (**a**) region-averaged monthly mean AI and (**b**) pentad mean AI in northern China for the period 1978–2005

increase afterward. The seasonal trend is consistent with monthly mean AI, though the pentad mean peak occur at the beginning of May rather in April like in Fig. 4a. In addition, the pentad mean AI exhibits a series of short-term fluctuations, which can be explained in combination with the analysis of regionally different natural and human factors.

The entire region is divided into three sub-regions by latitude and longitude: Northwest China (west of 100°E), North China (100°E-120°E) and Northeast China (east of 120°E, north of 40°N) (Fig. 1). Figure 5 shows seasonal variations in monthly mean AI and pentad mean AI in the three sub-regions of northern China for the period 1978–2005. Variation in North China throughout the year is similar to that of the whole study area. The winter mean AI values are significantly higher for Northeast China, especially in December and January, than those for Northwest China and North China. January has the highest value in Northeast China, followed by April, with December similar to March and May. Northwest China sub-region shows a peak in late spring and early summer, with the highest monthly average in May, and AI values from May to October are always higher than those in North China and Northeast China, indicating a higher dust AOD in summer.

According to Fig. 5b, the pentad mean AI of Northwest China sub-region increases rapidly beginning from the seventeenth pentad, similar to the seasonal variation in Northeast China sub-region; AI is always higher in Northwest China than in Northeast China and North China between the twenty-sixth and fifty-sixth pentads. An interesting phenomenon is that the AI of all three sub-regions converts seasonally in the twenty-second and sixty-first pentads each year, as indicated by the intersections of the three curves (Fig. 5b). The

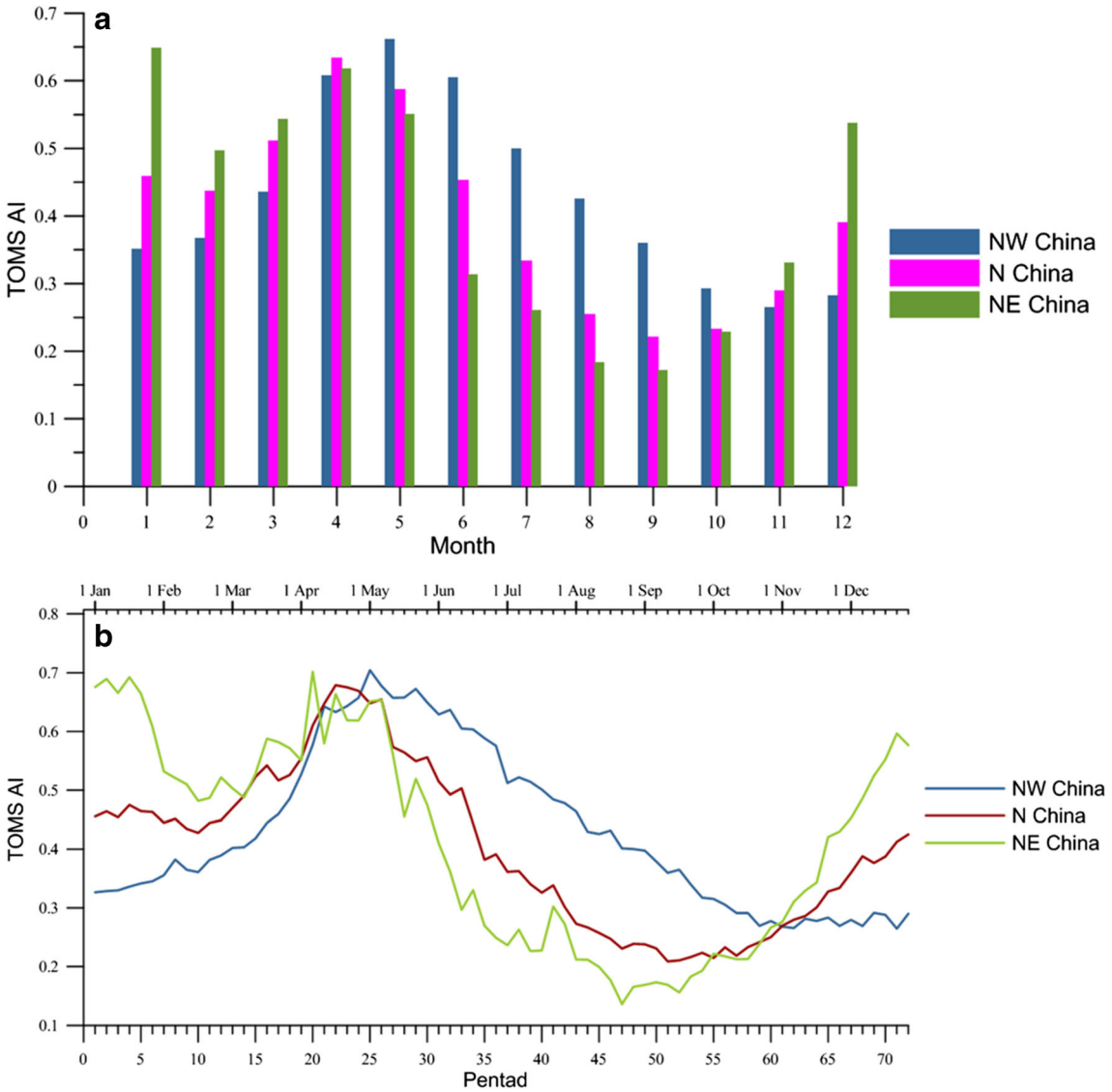

Fig. 5 Seasonal variations in (**a**) region-averaged monthly mean AI and (**b**) pentad mean AI in the three sub-regions of northern China for the period 1978–2005

earlier intersection time is the beginning of the summer mode when the pentad mean AI values rank in order of Northwest China > North China > Northeast China; and later intersection represents a shift to entry into winter mode when the pentad mean AI values rank in an opposite order of Northeast China > North China > Northwest China.

The differences of the regional and seasonal variations are related to climate and other natural conditions in each sub-region. The seasonal changes in the relative proportions of natural and anthropogenic aerosol emissions are also important. The reason that the mean AI values of the winter months and pentads are higher in Northeast China than in North China and Northwest China may be linked to carbonaceous aerosol emissions, and the stable atmospheric stratification during winter, as mentioned above. However, for Northwest China, anthropogenic aerosol emissions are low, and dust aerosols are difficult to be dislodged and transported under the stable atmospheric conditions typical of winter. Significant differences of pentad mean AI values in Northwest China from those in other sub-regions in summer may be explained by the heavy monsoon rainfall in North China and Northeast China, and the poor vegetation cover and strong upward air motion in Northwest China which are caused by extremely dry climate, bare ground, and local heating in the desert region.

It is worth noting that the emission of carbonaceous aerosols in North China should be higher than those in Northeast China in all seasons; however, the opposite is true for the mean AI, which may suggest the important influence of atmospheric stability in the lower troposphere in maintaining higher carbonaceous AOD in winter. In the summer half of the year, the lack of higher atmospheric stability conditions in Northeast China from mid-May to mid-October leads to pentad mean values of AI in North China being higher than those in Northeast China.

EOF analysis

EOF analysis was used to examine the leading modes and the time series of annual and spring mean AI in northern China. Cumulative variance contribution of the first three eigenvectors reaches 70.98 %, and focus was thus on analysis of the first three modes.

The first mode (EOF1), which represents a consistent variability in the whole area of northern China, explains 50.03 % of the total variance, indicating that it is the main mode of inter-annual variability of dust AOD in the study area (Fig. 6a). The positive values appear everywhere, and the centers of the positive values are located in the southern basins, Northeast China Plain and the regions surrounding the Bohai Sea. Overall, the EOF1 may show the dust transport mode of larger particles. As dust sources, the Taklimakan Desert and the Qaidam Basin increase the AI values in the southern basins of the study area, and the Horqin Sandy Land heightens the AI of the Northeast China Plain. Circumstances in the Bohai Sea are special, in that the larger-particle aerosol concentration in this region is greater than in other regions, possibly due to anthropogenic floating dust and carbonaceous aerosols in the densely populated region, and the salt aerosols or foam caused by shock waves in the Bohai Sea (Zhang et al. 2016), in addition to the influence of the natural dust particle transport.

The time series corresponding to EOF1 has a weak long-term upward trend over the period 1978–2005, consistent with the original AI series (Ren et al. 2014) (Fig. 6). From the time series, it can be seen that strong dust-prone events appear in 1993, 1996, 2001 and 2002, whereas 2000 is characterized by relatively fewer and weaker dust storms due to the more abundant precipitation. The weak increasing trend of the EOF1 may be attributed to severe droughts in the late 1990s and the first years of twenty-first century in North and Northeast China (Ren et al. 2005).

Variance of the second mode (EOF2) accounts for 14.40 % (Fig. 6b), and it exhibits a spatial pattern of north–south dipole distribution. The zero-value line distributes approximately along 34° N, and the positive values appears north of 34° N and negative values in the south, reflecting the reversal of the spatial distribution of AI from north to south in northern China. The implications of the north–south dipole distribution need to be investigated, but it may indicate a long-range transport mode of small dust particles.

The third mode (EOF3) explains 6.55 % of the total variance, and spatial distribution characteristics show a northwest–southeast "±" dipole pattern (Fig. 6c), with the zero-value line crossing southeastern Inner Mongolia to the center of Shanxi westward along 36° N, and negative values distributing in northwest of the study area. The negative-value center appears in the northwest, which contains extremely dry desert regions, and is prone to dust weather. The pattern may have been related to the combined influences from naturally occurred dust storms, floating dust and blowing sand in the arid regions. The time series of the EOF3 indicates a consistent variability with the EOF1 before the mid-1990s, and an opposite phase afterward. This may be related to the enhanced anthropogenic role in the last decade in the eastern regions, which may have increased the concentration of the floating dust and carbonaceous aerosols.

Spatial patterns of the leading modes for spring mean AI in northern China are shown in Fig. 7a. The cumulative contribution of the first three modes accounts for 70.87 %, and the first two modes were briefly analyzed here.

The EOF1explains 57.90 % of the total variance, and the spatial distribution is characterized by positive values of the whole study area, reflecting spatial consistency of temporal variability of AOD in northern China. The spatial pattern and the time series are very similar to those of the EOF1 of annual mean AI, probably indicating the influence of naturally originated larger-particle aerosols in spring.

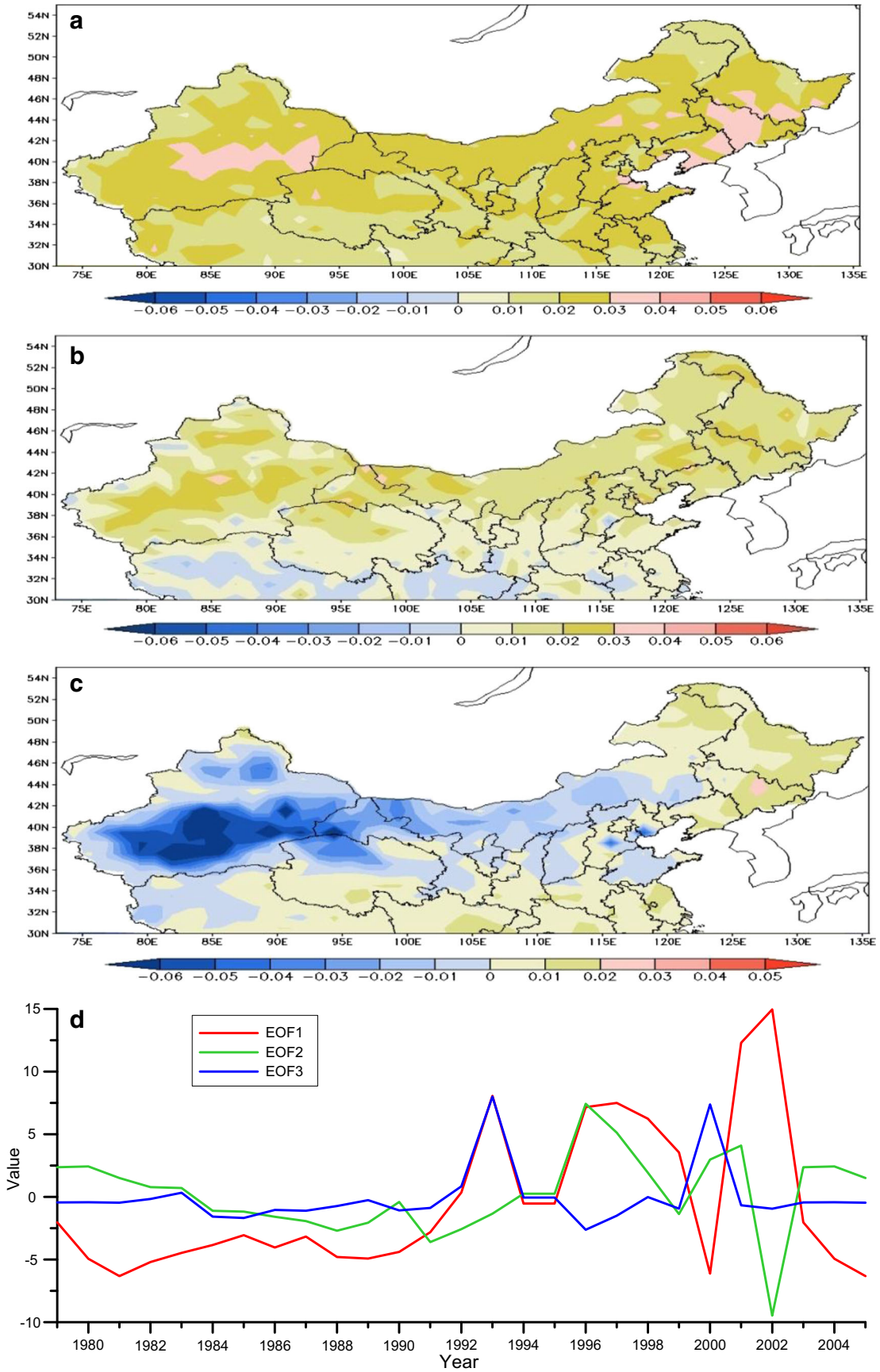

Fig. 6 Spatial distributions of the first three EOFs (**a**, **b**, **c**) of annual mean AI and their time coefficient series (**d**)

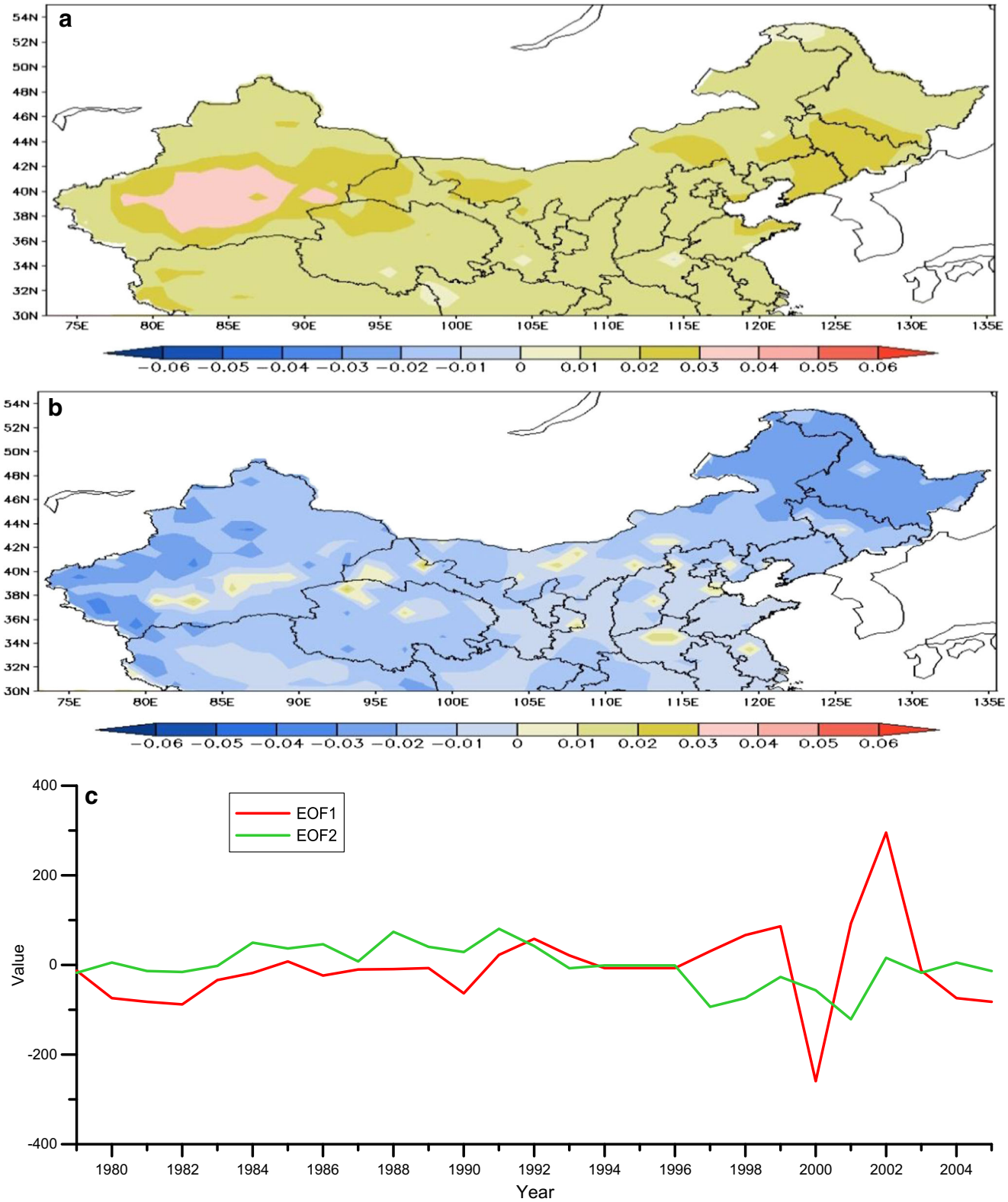

Fig. 7 Spatial distributions of the first two EOFs (**a, b**) of spring mean AI and their time coefficient series (**c**)

The EOF2 explains 12.97 % of the total variance (Fig. 7b). In most parts of northern China, the spatial distribution of the EOF2 is characterized by the identically negative values, with the negative eigenvalues being greater in the western part of the northeast and northern part of the northwest (Fig. 7b).

Conclusions and discussion

Conclusions

This paper analyzes the tempo-spatial characteristics of dust and carbonaceous AOD index (AI) series in northern China based on daily data of TOMS AOD from NASA during 1978–2005. The conclusions are as follows:

Significantly higher AI values (>0.8) occur in the western desert regions including the Taklimakan Basin, the Qaidam Basin and west of Gansu province; the areas with the second highest values (0.5–0.8) are in the western part of Inner Mongolia. The AI values of the Junggar Basin, northern part of the Loess Plateau and the North and Northeast China Plains register higher AI values, usually 0.4–0.7. The smallest AI values appear in the junction belt of Sichuan province, Qinghai province and Tibet Autonomous Region, and the western Altai and Tianshan Mountains.

The seasonal mean AI in the northern China is markedly higher in spring and summer than in other seasons. The range and value of AI are highest in spring; AI is significantly weaker during the summer monsoon season, especially in North China and Northeast China, but still maintains high levels in the deserts of Northwest China. In most areas, AI values reach the annual minimum in autumn, but remain higher in the southern Xinjiang; in winter, the Northwest arid area represented by the Taklimakan Desert reaches the annual minimum, but the average AI value in the eastern monsoon region is significantly higher than in summer or autumn, particularly in the north of Northeast China.

AI reaches high values in the entire northern region in spring and early summer (March–June), with the highest values being in April and May; lower values occur in autumn (September–November), and the lowest values in October. Winter is the season with the second-highest AI values, after spring; AI values in summer are higher than those in fall. In the study area as a whole, the mean AI undergoes rapid growth from the tenth to the twenty-fifth pentad, and then begins to decline rapidly until the fifty-seventh pentad, when it reaches its lowest level, followed by a slow increase.

Of all sub-regions, North China has a variation throughout the year similar to that of the whole study area. The average AI values of Northeast China are significantly higher than in Northwest China and North China in winter, especially in December and January. The peaks in Northwest China occur in late spring and early summer. There are the periods for the three sub-regions to convert seasonally in the twenty-second and sixty-first pentads, with April 16–20 marking the entrance into the summer mode, and November 1–5 into the winter mode.

Discussion

The AI index can be combined with the dust deposition flux to obtain the relationship between the two in order to use the AI to estimate the dust deposition flux in the vast arid areas. The dust deposition is high in the arid dust-prone areas, and the dust flux is positively correlated with dust weather frequency (Pye and Zhou 1989; Pye 2015; Nihlén et al. 1995; McTainsh et al. 1997; Li et al. 2008). Therefore, the AI index has potential to be used for obtaining a high-resolution spatial and temporal pattern of the dust deposition flux in northern China, which will be helpful for understanding current and paleo-environmental issues in the region.

The thick loess stratum in northern China especially in the Loess Plateau has been assumed to be formed through a large amount of deposition of mineral dust carried by dust storms in the Quaternary period, probably due to the strengthening of the East Asian winter monsoon in East Asia (Liu 1985; Liu et al. 1991; Nihlén et al. 1995; Zhang 2001; Liu et al. 2004; Qin et al. 2005; Sun et al. 2007). The thickest loess was found in the Loess Plateau, and the thinner loess was also found in the Kunlun Maintains and some places of Northeast China (Liu 1985; Pye and Zhou 1989). Liu et al. (2014) even found significant aeolian features through analyzing the lake sediment of Dongdao Island in the South China Sea, and attributed the aeolian sediments to dust deposition from the arid inland Asia.

Except for other conditions like vegetation distribution, the spatial difference of dust deposition flux in the past would be an important determinant for the varied loess thickness in northern China. Overall, the AI series and ground-based observation records exhibit good consistency, especially in arid and semi-arid regions (Ren et al. 2014). Satellite remote-sensing reconstructed results have advances over the ground-based observations, because they could better reflect the atmospheric dust deposition flux. The AI index can thus be used to estimate the current dust deposition flux, which might be further used in combination with the data of actual loess thickness and distribution to verify and develop the theory of the loess formation and evolution.

Monsoon might have affected the seasonal and geographical distribution of dust flux and deposition. Modern observational studies show that stronger East Asian winter monsoon conduces to dust weather occurrence in winter and next spring, and the stronger summer monsoon reduces the frequency of dust weathers (Ye et al. 2000; Wang et al. 2000; Wu et al. 2010). It would be interesting to check whether or not the relationship is still hold for AI and monsoon strength. If so, the AI data and the reconstructed dust flux data could be useful for understanding the variability of Asian winter monsoon and its influence on dust deposition.

Of course, the high carbonaceous aerosol concentration in winter in some regions, such as the northern part of the

Northeast China Plain, suggests that AI is not a completely accurate representation of dust aerosols. In regions with increasing anthropogenic emissions of carbonaceous aerosols, the AI data and the analysis results need to be carefully treated for presenting the dust AOD or dust flux. The anthropogenic contamination of carbonaceous aerosols has to be removed if the AI index is to be used in accurately reconstructing aeolian dust flux, and in understanding the dynamics of the China Loess deposition and evolution in the past.

Acknowledgments This work is financially supported by the China Natural Science Foundation (Fund No: 41575003) and the Ministry of Science and Technology of China (Fund No: GYHY201206012). We thank Zhang, F. X. for supplying the TOMS AI data.

References

Bond TC, Streets DG, Yarber KF, Nelson SM, Woo JH, Klimont Z (2004) A technology-based global inventory of black and organic carbon emissions from combustion. J Geophys Res-Atmos 109(D14)

Chu DA, Kaufman YJ, Ichoku C, Remer LA, Tanré D, Holben BN (2002) Validation of MODIS aerosol optical depth retrieval over land. Geophys Res Lett 29(12)

Deng ZQ, Han YX, Bai HZ, Zhao TL (2009) Analysis of the causes for change of dust aerosol concentration in desert regions. China Envi Sci 29(12):1233–1238

Ding K, Liu JP (2011) Spatial distribution and dynamic changes of sand storm in northern China in recent 50 years. J Arid Land Resour Envi 25(4):116–120

Ding ZL, Sun JM, Liu TS (1999) Sedimentological indices as indicators of the relationship between deserts and Loess. Sci China 29(1):82–87

Fang ZY, Wang W (2006) Characteristics of China dust storm in 2002. J Appl Meteor Sci 14(5):513–522

Fang ZY, Zhang YG, Zheng XJ, Cao YC (2001) The method for monitoring dust devil using satellite and preliminary results [J]. Quate Sci 1:006

Fang XM, Han YX, Ma JH, Song LC, Yang SL, Zhang XY (2003) Dust characteristics and loess deposition over the Qinghai-Tibetan plateau. Chin Sci Bull 49(11):1084–1090

Gao ZT, Zhang RJ, Su LX (2009) Characteristic analysis of atmospheric black carbon aerosols in Changchun in autumn and winter. Plateau Meteorol 28(4):803–807

Ke F, Hui-Jun W (2006) Interannual variability of dust weather frequency in Beijing and its global atmospheric circulation. Chin J Geophysics-Chinese Edition (in Chinese) 49(4):1006–1014

Levy RC, Remer LA, Dubovik O (2007) Global aerosol optical properties and application to moderate resolution imaging spectroradiometer aerosol retrieval over land. J Geophys Res-Atmos 112(D13)

Li C, Mao J, Lau KHA, Chen JC, Yuan Z, Liu X et al (2003) Characteristics of distribution and seasonal variation of aerosol optical depth in eastern China with MODIS products. Chin Sci Bull 48(22):2488–2495

Li SY, Lei JQ, Xu XW, Wang D, Wang LH, Li YD (2006) Features of sandstorms in hinterland of Taklimakan Desert a case of Tazhong area. Ziran Zaihai Xuebao/ J Nat Dis 15(2):14–19

Li X, Wang S, Duan L, Hao J, Li C, Chen Y, Yang L (2007) Particulate and trace gas emissions from open burning of wheat straw and corn Stover in China. Environ Sci Technol 41(17):6052–6058

Li JC, Dong ZB, Wang XM (2008) Amount of spring dustfall and its environmental significance in east part of northern China. J Desert Res 28(2):195–201

Lin II, Chen JP, Wong GT, Huang CW, Lien CC (2007) Aerosol input to the South China Sea: results from the MODerate resolution imaging spectro-radiometer, the quick scatterometer, and the measurements of pollution in the troposphere sensor. Deep-Sea Res II Top Stud Oceanogr 54(14):1589–1601

Liu DS (1985). Loess and environment in China. Beijing: Science Press. (in Chinese)

Liu D, Ding Z, Guo Z (1991) Loess, environment, and global change. Science Pr.

Liu LY, Shi PJ, Gao SY, Zou XY, Erdon H, Yan P, Zhang CL (2004) Dustfall in China's western loess plateau as influenced by dust storm and haze events. Atmos Environ 38(12):1699–1703

Liu Y, Sun L, Zhou X, Luo Y, Huang W, Yang C, Wang Y, Huang T (2014) A 1400-year terrigenous dust record on a coral island in South China Sea. Sci Report 2014. doi:10.1038/srep04994

Lu Z, Zhang Q, Streets DG (2011) Sulfur dioxide and primary carbonaceous aerosol emissions in China and India, 1996–2010. Atmos Chem Phys 11(18):9839–9864

Martonchik JV, Diner DJ, Crean KA, Bull MA (2002) Regional aerosol retrieval results from MISR. IEEE Trans Geosci Remote Sens 40(7): 1520–1531

McTainsh GH, Nickling WG, Lynch AW (1997) Dust deposition and particle size in Mali, West Africa. Catena 29(3):307–322

Mi W, Li Z, Xia X, Holben B, Levy R, Zhao F, Cribb M (2007) Evaluation of the moderate resolution imaging spectroradiometer aerosol products at two aerosol robotic network stations in China. J Geophys Res Atmos 112:D22S08

Nihlén T, Mattsson JO, Rapp A, Gagaoudaki C, Kornaros G, Papageorgiou J (1995) Monitoring of Saharan dust fallout on Crete and its contribution to soil formation. Tellus B 47(3):365–374

Novakov, T., & Penner, J. E. (1993). Large contribution of organic aerosols to cloud-condensation-nuclei concentrations.

Pye K (2015) Aeolian dust and dust deposits. Elsevier

Pye K, Zhou LP (1989) Late Pleistocene and Holocene aeolian dust deposition in North China and the Northwest Pacific Ocean. Palaeogeogr Palaeoclimatol Palaeoecol 73(1):11–23

Qian ZA, Shong MH, Li WY (2002) Analyses on distributive variation and forecast of sand-dust storms in recent 50 years in North China. J Desert Res 2:106–111

Qian ZA, Cai Y, Liu JT, Li DL, Liu ZM, Song MH (2004) Some advances in dust storm researches in northern China. J Arid Land Resour Envi 18(1):1–8

Qin X, Cai B, Liu T (2005) Loess record of the aerodynamic environment in the East Asia monsoon area since 60,000 years before present. J Geophys Res Solid Earth 110(B1)

Qiu XF, Zeng Y, Miao QL (2001) Temporal-spatial distribution as well as tracks and source areas of sand-dust storms in China. Acta Geogr Sin (Chin Ed) 56(3):322–330

Ren, G.Y., Guo, J., Xu, M.Z., Chu, Z.Y., Zhang, L., Zou, X.K., & Liu X.N, L. (2005). Climate changes of China's mainland over the past half century. Acta Meteorol Sin, 63(6), 942–956.

Ren XY, Ren GY, Wei MJ (2014) Comparison between TOMS optical depth index of aerosol and dust weather frequency in northern China. Arid Zone Res (in Chin) 31(5):874–881

Seinfeld JH, Pandis SN (2016) Atmospheric chemistry and physics: from air pollution to climate change. John Wiley & Sons

Streets DG, Gupta S, Waldhoff ST, Wang MQ, Bond TC, Yiyun B (2001) Black carbon emissions in China. Atmos Environ 35(25):4281–4296

Streets DG, Yu C, Wu Y, Chin M, Zhao Z, Hayasaka T, Shi G (2008) Aerosol trends over China, 1980–2000. Atmos Res 88(2):174–182

Sun J, Zhang M, Liu T (2001) Spatial and temporal characteristics of dust storms in China and its surrounding regions,

1960–1999: relations to source area and climate. J Geophys Res-Atmos 106(D10):10325–10333

Sun DH, Lu HY, Sun YB (2007) Grain-size and dust accumulation rate of late Cenozoic Aeolian deposits and the inferred atmospheric circulation evolutions. Quat Sci 27(2):251–262

Torres O, Bhartia PK, Herman JR, Ahmad Z, Gleason J (1998) Derivation of aerosol properties from satellite measurements of backscattered ultraviolet radiation: theoretical basis. J Geophys Res-Atmos 103(D14):17099–17110

Torres O, Bhartia PK, Herman JR, Sinyuk A, Ginoux P, Holben B (2002) A long-term record of aerosol optical depth from TOMS observations and comparison to AERONET measurements. J Atmos Sci 59(3):398–413

Wang ZH (2003) The research on the aerolion dust deposition monitoring. J Arid Lnad Resour Envi (in Chin) 17(1):54–59

Wang, J.G., & Ren, G.Y., (2003). Atlas of dust climate in China. Meteorological Press (in Chinese), Beijing.

Wang SG, Dong GR, Yang DB, Jin J, Shang KZ (1996) A study on sand-dust storms over the desert region in North China. J Nat Dis 5(2):86–94

Wang SG, Dong GG, Chen HZ, Li XL, Jin J (2000) Advances in studies of sand-dust storms of China. J Desert Res (in Chin) 20(4):349–356

Wang Z, Wang T, Gao R, Xue L, Guo J, Zhou Y, Zhou X (2011) Source and variation of carbonaceous aerosols at mount tai, North China: results from a semi-continuous instrument. Atmos Environ 45(9): 1655–1667

Wang Z, Wang T, Guo J, Gao R, Xue L, Zhang J, Wang W (2012) Formation of secondary organic carbon and cloud impact on carbonaceous aerosols at mount tai, North China. Atmos Environ 46:516–527

Washington R, Todd M, Middleton NJ, Goudie AS (2003) Dust-storm source areas determined by the total ozone monitoring spectrometer and surface observations. Ann Assoc Am Geogr 93(2):297–313

Wu Y, Zhang R, Han Z, Zeng Z (2010) Relationship between east Asian monsoon and dust weather frequency over Beijing. Adv Atmos Sci 27:1389–1398

Xu J, Bergin MH, Yu X, Liu G, Zhao J, Carrico CM, Baumann K (2002) Measurement of aerosol chemical, physical and radiative properties in the Yangtze delta region of China. Atmos Environ 36(2):161–173

Yang Y, Wang J, Tian M, Chen X (2012) Distribution characteristics and research method of sandstorms in China. Des Rese (in Chin) 32: 465–472

Ye DZ, Chou JF, Liu JY (2000) Causes of sand-stormy weather in northern China and control measures. Acta Geogr Sin Chin Ed 55(5): 513–521

Zhang XY (2001) Source distributions, emission, transport, deposition of Asian dust and loess accumulation. Quat Sci (in Chin) 21(1):29–40

Zhang L, Ren GY (2003) Change in dust storm frequency and the climatic controls in northern China. Acta Meteorol Sin 61(6): 744–750

Zhang X, Arimoto R, An Z, Chen T, Zhang G, Zhu G, Wang X (1993) Atmospheric trace elements over source regions for Chinese dust: concentrations, sources and atmospheric deposition on the loess plateau. Atmospheric environment. Part A Gen Top 27(13):2051–2067

Zhang Q, Streets DG, Carmichael GR, He KB, Huo H, Kannari A, Chen D (2009) Asian emissions in 2006 for the NASA INTEX-B mission. Atmos Chem Phys 9(14):5131–5153

Zhang N, Qin Y, Xie SD (2013a) Spatial distribution of black carbon emissions in China. Chin Sci Bull 58(19):1855–1864

Zhang Y, Shao M, Lin Y, Luan S, Mao N, Chen W, Wang M (2013b) Emission inventory of carbonaceous pollutants from biomass burning in the Pearl River Delta region, China. Atmos Environ 76:189–199

Zhang J, Chen J, Xia X, Che H, Fan X, et al (2016) Heavy aerosol loading over the Bohai Bay as revealed by ground and satellite remote sensing. Atmospheric Environment 124(B):252–261

Zhou ZJ (2001) Blowing-sand and sandstorm in China in recent 45 years. Quat Sci (in Chin) 21(1):9–17

Zhuang G, Guo J, Yuan H, Zhao C (2001) The compositions, sources, and size distribution of the dust storm from China in spring of 2000 and its impact on the global environment. Chin Sci Bull 46(11):895–900